

# TRACTRLFUSION: A GPT-BASED MULTI-CRITIC POLICY FUSION FRAMEWORK FOR FIBER TRACTOGRAPHY

Ankita Joshi<sup>1</sup>, Ashutosh Sharma<sup>1</sup>, Anoushkrit Goel<sup>1</sup>, Ranjeet Ranjan Jha<sup>2</sup>,  
Chirag Ahuja<sup>3</sup>, Arnav Bhavsar<sup>1</sup>, Aditya Nigam<sup>1</sup>

<sup>1</sup> IIT Mandi, <sup>2</sup> IIT Patna, <sup>3</sup> PGIMER Chandigarh

## ABSTRACT

Tractography plays a pivotal role in the non-invasive reconstruction of white matter fiber pathways, providing vital information on brain connectivity and supporting precise neurosurgical planning. Although traditional methods relied mainly on classical deterministic and probabilistic approaches, recent progress has benefited from supervised deep learning (DL) and deep reinforcement learning (DRL) to improve tract reconstruction. A persistent challenge in tractography is accurately reconstructing white matter tracts while minimizing spurious connections. To address this, we propose TractRLFusion, a novel GPT-based policy fusion framework that integrates multiple RL policies through a data-driven fusion strategy. Our method employs a two-stage training data selection process for effective policy fusion, followed by a multi-critic fine-tuning phase to enhance robustness and generalization. Experiments on HCP, ISMRM, and TractoInferno datasets demonstrate that TractRLFusion outperforms individual RL policies as well as state-of-the-art classical and DRL methods in accuracy and anatomical reliability.

**Index Terms**— Diffusion MRI, Tractography, Reinforcement Learning, Transformers

## 1. INTRODUCTION

White matter tractography[1] is a key technique to study brain structural connectivity, neurological disorders, and to support precise neurosurgical planning [2]. It enables *in vivo* and non-invasive mapping of white matter pathways using diffusion MRI (dMRI) data. dMRI captures the anisotropic diffusion (movement) of water molecules within white matter tissue, as water diffuses more readily along the axonal fibers. This directional dependence is typically modeled using fiber orientation distribution functions (fODFs), allowing inference of white matter pathways. Traditional tractography algorithms are generally categorized as *deterministic*, *probabilistic*, and *global* approaches. *Deterministic methods*[3, 4] reconstruct streamlines by following the principal diffusion direction at each step, but often fail in regions with crossing, branching, or other complex fiber configurations. In contrast, *probabilistic methods*[5] estimate a distribution of possible

pathways at each step, improving coverage, but at the cost of increased false positives (FPs). Global methods[6] attempt to handle the FP-FN trade-off in tractography[7, 8], improving overall consistency but at the cost of high computational cost and limited generalizability. Supervised Learning based methods rely on ground-truth tracts for training. For example, a Random Forest Classifier[9] predicts the next streamline direction from a set of candidate directions and past estimated steps. Similarly, DL methods such as Learn-to-Track[10] and DeepTract[11] formulate tractography as a sequential decision making task, employing GRUs to model streamline paths and probabilistic fiber orientation distributions, respectively. In parallel, DRL methods[12, 13, 14, 15] learn tractography policies through exploration rather than direct supervision.

Interestingly, we observe a similar FP-FN trade-off among both deterministic and stochastic RL policies. This observation motivates our investigation of the fusion of RL policies to improve tractography performance, a strategy that has proven to be effective in other domains, such as robotics and AI games to improve generalization and robustness[16, 17]. Traditional ensemble strategies for RL policy, including decision-level aggregation (e.g., voting or averaging), often fail to capture semantic context or state history. Conversely, more complex ensemble methods, such as Ensemble Policy Gradient or hierarchical ensembles, introduce significant system complexity due to agent synchronization, parameter sharing, and joint optimization requirements, making them difficult to implement, debug, and maintain.

To address these challenges, we propose **TractRLFusion** (Fig. 1), a data-driven fusion framework to combine multiple RL policies in tractography. In this work:

- We introduce **TractRLFusion**, a novel GPT-based policy fusion framework that integrates **Episodic Data Selection (EDS)** to select tract-specific trajectories with anatomical precision, enabling data-driven fusion.
- We propose **Multi-Critic Policy Fine-Tuning (MCPFT)** to enhance policy fusion, achieving **robust**, **scalable**, and **generalizable** tractography across diverse datasets.
- Extensive *comparative* evaluation against state-of-the-art tractography methods demonstrate its **superior performance**, **effectiveness**, and generalizability.

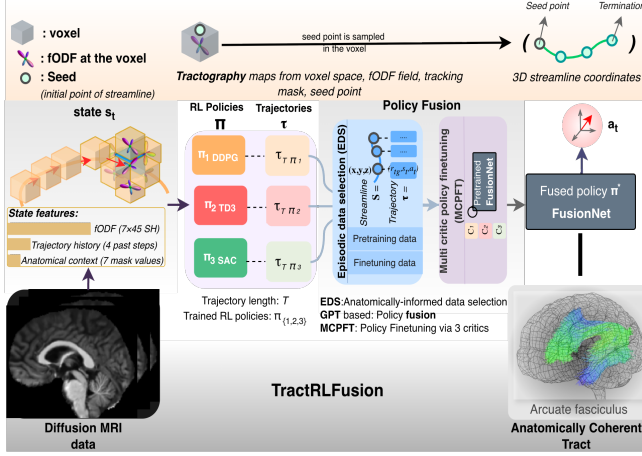


**Fig. 1: TractRLFusion:** An RL policy fusion framework for tractography, comprising EDS, FusionNet and MCPFT.

To our knowledge, this is the first policy-fusion framework for tractography. **Code will be released on GitHub.**

## 2. METHODOLOGY

We fuse three independently trained policies, namely TD3 [18], SAC [19], and DDPG [16], to combine their complementary strengths in tractography. While SAC learns in an exploration-driven manner, resulting in higher tract coverage but increased false positives, TD3 and DDPG exhibit more conservative tracking behavior, yielding lower coverage with fewer false positives, as shown in Table 3. The TractRLFusion framework comprises three key components: Episodic Data Selection (**EDS**), **FusionNet**, and Multi-Critic Policy Finetuning (**MCPFT**). To enable data-driven fusion, we sample trajectories from trained RL policies, where a trajectory represents a sequences of state, action, and return-to-go tuples obtained from an RL policy. A trajectory of length  $T$  is defined as:  $\tau = (s_0, a_0, r_{t_0}, s_1, \dots, s_T, a_T, r_{t_T})$ .

**(i)** EDS samples a mix of trajectory data from each of the three policies to train FusionNet. **(ii)** FusionNet is then trained in two stages on EDS data to learn the fusion policy. **(iii)** Finally, the FusionNet policy is refined using MCPFT to enhance stability and generalization.

FusionNet learns a tract-specific policy for each targeted white matter bundle. To this end, we train and evaluate our policies within tract-specific masks from [15]. Among the major tracts, we focus on the occipital and pre/post central gyri regions of the Corpus Callosum (CC), the left and right Corticospinal Tract (CST), the Arcuate Fasciculus (AF), and the Cingulum (CG), following previous work[13].

**Tract-Specific RL policy Training:** Training is conducted through exploration in an environment similar to [12], but constrained within tract-specific masks of **five training subjects** from the TractoInferno dataset[20] (Table 1). The reward is defined as the product of the action vector's ( $\vec{a}_t$ ) alignment with the most aligned fODF peak ( $p$ ) and its dot product with the previous tracking direction ( $\vec{u}_{t-1}$ ):

$$r_t = \left| \max_{p_i} (\vec{p}_i \cdot \vec{a}_t) \right| \times (\vec{a}_t \cdot \vec{u}_{t-1}) \quad (1)$$

**Episode termination conditions** are **(i)** exceeding 530 steps ( $\approx 200$  mm fiber), **(ii)** leaving the tract mask, or **(iii)** an angle  $> 60$  with the previous segment. Subsequent sections describe each component of Tract-RLFusion in detail.

### 2.1. Episodic Data Selection

It is the data preparation process for the pre-training and finetuning stages of FusionNet model. It involves following steps:

**(i)** Tracking is performed using each trained policy (TD3, SAC, and DDPG) from a common batch of neighboring seed points sampled from the tract mask of a given subject. This produces streamlines  $\{(x, y, z)\}$  along with their corresponding trajectory tuples  $(s, a, r_{tg})$ .

**(ii)** Trajectories containing fewer than 47 transitions (equivalent to approximately 20mm for a 1mm<sup>3</sup> voxel size and 0.375 step size) are filtered-out. The remaining trajectories then undergo batch-wise **across-policy** and **within-policy** selection for subsequent processing.

**(iii) Within-policy selection:** Fifteen reference streamlines are selected from the atlas tract[21] using the farthest streamline sampling. For each policy, we filter streamlines to retain only the trajectories that lie within a 5mm MDF (mean direct flip) distance [22] from the reference streamlines, thus selecting the most anatomically accurate trajectories.

**(iv) Across policy selection** selects one policy out of the three (TD3, SAC, DDPG), based on the maximum expected Q-value (normalised to incorporate different scales) of its MDF-filtered trajectories. These trajectories are selected for the finetuning dataset. In contrast, for the pretraining dataset, Q-value-based selection is performed directly on the unfiltered trajectories.

Neighboring seed points are selected in each batch, enabling EDS to select the best trajectories from all regions of the given tract. This process is repeated across all tracts of the five training subjects, resulting in approximately 150000 pre-training and 50000 finetuning trajectories after length-based and random selection. In particular, the pretraining dataset comprises trajectories from all tracts, whereas the **finetuning data consists of tract-specific trajectories**.

### 2.2. FusionNet (Architecture and Training)

Central to our framework, FusionNet is a 4-layer GPT [23] (one attention head, 128-dim embeddings, context length 40, ReLU activation, and dropout rate of 0.1) that models RL trajectories as sequences. It undergoes general pretraining and tract-specific fine-tuning on expert trajectories from EDS. Specifically, the first three layers are trained on mixed trajectories from the EDS pretraining data over 30 iterations, while the final layer is fine-tuned for 10 iterations using tract-specific trajectories from the EDS finetuning data. This two-stage training strategy (Table 2) is designed to first capture

broad trajectory patterns and subsequently adapt to the fine-grained tract-specific details. We employ a five-step angular loss ( $\mathcal{L}_{dist_{cos}}$ ) between predicted ( $\hat{\mathbf{a}}$ ) and actual ( $\mathbf{a}$ ) actions:

$$\mathcal{L}_{dist_{cos}} = \sum_{t=2}^{l_{context}-2} \left( \sum_{i=-2}^2 \cos^{-1}(\mathbf{a}_{t+i} \cdot \hat{\mathbf{a}}_{t+i}) \right) \quad (2)$$

The model was trained with AdamW optimizer, hyperparameters tuned to maximize Accumulated sum of rewards and Dice Scores. Additional training with supervised loss (Eq. 2) led to performance saturation, showing limited improvement.

### 2.3. Multi-critic Policy Fine-tuning (MCPFT)

We fine-tune FusionNet using MCPFT in an actor-critic setup with critic networks derived from SAC, DDPG, and TD3.

$$\mathcal{L}_{actor} = \mathcal{L}_{dist_{cos}} + \sum_{k=1}^{K=3} \underbrace{\left[ - \sum_{t=0}^{l_{context}} Q_{(\pi_k)}^C(s_t, \hat{a}_t) \right]}_{\mathcal{L}_{critic,k}} \quad (3)$$

The actor (**FusionNet**) is optimized using the composite loss  $\mathcal{L}_{actor}$  (Eq. 3), which combines the supervised loss  $\mathcal{L}_{dist_{cos}}$  with the aggregated loss from our  $K = 3$  critics, where each  $\mathcal{L}_{critic,k}$  is formulated to maximize the critics' value estimates (Eq. 3). Standalone aggregated critic loss ( $\sum_{k=1}^3 \mathcal{L}_{critic,k}$ ) caused a performance drop after a few updates, followed by saturation below the prior levels. Our observations during training indicate the ability of  $\mathcal{L}_{dist_{cos}}$  to preserve prior actor knowledge, while the critic term further refines its policy. We observed that delayed critic updates prevent saturation from unstable value estimates. Training parameters are summarized in Table 2.

### 2.4. Tracking Process

Using the FusionNet policy, tracking is performed for different tracts within their respective tracking masks, by seeding at 7 seeds per voxel. Return-to-go ( $r_{t_0}$ ) is initialized to 300 for FusionNet, and dataset-specific step sizes (0.375mm for TractoInferno, 0.468mm for HCP, 0.75mm for ISMRM) are set. As a postprocessing step, tract filtering is performed using Fast Streamline Search [24] with atlas reference tracts [25].

Category	Details
<b>State Features</b>	<ul style="list-style-type: none"> <li>- 45 SH coefficients (6 neighbors+1)</li> <li>- Last 4 past directions (12 values)</li> <li>- Tract mask value (6 neighbors+1)</li> <li>- Concatenated to: 334 dimensions</li> </ul>
<b>Architectures (Actor, Critics)</b>	<ul style="list-style-type: none"> <li>- 3-layer ReLU-activated FCNNs</li> <li>- Neurons per hidden layer: 1024</li> </ul>
<b>Train Data [20]</b>	<ul style="list-style-type: none"> <li>- IDs: 1030, 1079, 1119, 1180, 1198</li> </ul>
<b>Hyperparameters</b>	<ul style="list-style-type: none"> <li>- Batches: 50 per subject</li> <li>- Batch size: 4096 transitions</li> <li>- Seeding: 7/voxel; Step size: 0.375</li> </ul>
<b>Policy Hyperparameters</b>	<ul style="list-style-type: none"> <li>- <b>TD3</b>: <math>\eta = 8.56e-6</math>, <math>\sigma = 0.334</math>, <math>\gamma = 0.776</math></li> <li>- <b>SAC</b>: <math>\eta = 3.7e-5</math>, <math>\sigma=0.4</math>, <math>\gamma=0.89</math>, <math>\alpha=0.076</math></li> <li>- <b>DDPG</b>: <math>\eta = 8.56e-6</math>, <math>\sigma = 0.35</math>, <math>\gamma = 0.5</math></li> </ul>

**Table 1:** Summary of Features, Architecture, Train Subjects, and Hyperparameters for training Tract-specific RL policies.

Category	Details
<b>FusionNet</b> Training	<ul style="list-style-type: none"> <li>- Optimizer: AdamW (<math>\eta: 1e-4</math>)</li> <li>- Batch Size: 128; Updates/iter: 1e4</li> <li>- Iters: 30(General), 10(Tract-specific)</li> <li>- Warmup-Steps: 1e4</li> </ul>
<b>MCPFT-based</b> Finetuning	<ul style="list-style-type: none"> <li>- <math>\eta: 1e-4</math> ; Batch Size: 512 ; Iters: 25</li> <li>- Updates/iter: 1000 (actor), 1 (critic)</li> </ul>

**Table 2:** Summary of FusionNet training parameters.

## 3. EXPERIMENTS AND RESULTS

This section presents evaluation on test subjects from TractoInferno (1160, 1078, 1061, 1159, 1171), HCP (930449, 959574, 992774, 987983) and ISMRM. We compare with: Classical DET [1] and PROB (iFOD1) [26]; RL policies SAC, TD3, and DDPG[12, 13] employed in TractRLFusion, and their decision-level ensembles  $\pi_{maxQ}$  (Max Q-value action) and  $\pi_{Avg}$  (average of actions), TractSeg [27] and [15], incorporating SAC (best performing) in their framework (TRLF<sub>S</sub>). Since PROB contributed to create TractoInferno ground truth, it may be inherently favored. Moreover, reference streamlines for HCP [27] are made using iFOD2, a close successor of PROB. Hence it is evaluated on ISMRM. TractOracle [28] was left out, as it is tailored for WM/GM-interface seeding. Comparative analysis reveal the following notable insights:

- Our FusionNet model consistently ranks best across all datasets and tracts as shown in Table 3.
- Fusion policy (FusionNet) outperforms individual RL policies (SAC, TD3, DDPG) and their RL-Ensemble methods ( $\pi_{maxQ}$  and  $\pi_{avg}$ ). Individual RL policies show a high OR-OL tradeoff with SAC achieving highest OL with worst OR, and DDPG and TD3 achieving low OL and OR. The Ensemble's Q-value approach yields sub-optimal tracking, while FusionNet's learned policy better balances OL-OR trade-offs, resulting in the **best Dice**.
- FusionNet\* (FusionNet tested on TractSeg masks [27]) surpasses TractSeg across all HCP tracts, e.g., achieving a Dice score of 74.1 versus TractSeg's 70.9 for AF, demonstrating superior tracking even within TractSeg's masks.
- FusionNet\* and TractSeg achieve highest scores on HCP, as TractSeg was trained on HCP data to obtain those masks which were also involved in making reference streamlines of HCP. However, masks from [15] were available for all three datasets (TractoInferno, HCP, and ISMRM), preferred for a consistent comparison across these datasets. FusionNet's superior performance within both masks demonstrates its robustness to variations in mask quality for tract-specific tractography.
- Spurious connections made by SAC and PROB in left CG and CC\_Oc encircled in red (Fig. 2(a,b)) show lower OR by our method, consistent with the scores in table 3.
- In Fig. 2(a), PROB struggles to reconstruct upper portion of CST right, at pyramidal decussation (intersection of left & right CST) compared to FusionNet.
- Similar visual trend was observed in these tracts for other subjects, but we limit for brevity.

(a) CG and CST/PYT

Data	Algorithm	CG			CST/PYT		
		Dice↑	OL↑	OR↓	Dice↑	OL↑	OR↓
HCP	DET	53.9	44.1	18.9	62.9	51.8	11.7
	SAC	56.2	47.3	20.2	67.7	60.8	17.4
	DDPG	48.0	35.8	12.8	66.1	60.4	20.4
	TD3	49.2	37.5	14.7	55.7	46.2	15.8
	TRLF <sub>S</sub>	54.0	41.6	12.3	61.6	54.1	15.7
	$\pi_{maxQ}$	56.3	47.5	20.7	67.9	59.5	14.9
	$\pi_{avg}$	56.0	46.6	19.6	69.2	63.7	17.6
	<b>FusionNet</b>	<b>56.6</b>	47.2	19.2	<b>69.4</b>	62.5	17.0
	TractSeg	76.8	73.1	17.2	80.8	73.2	7.8
TractInferno	<b>FusionNet*</b>	<b>77.0</b>	86.7	38.2	<b>82.2</b>	79.8	14.4
ISM RM	DET	59.7	56.8	33.0	71.5	77.8	39.8
	SAC	63.1	70.9	55.9	73.0	70.3	22.0
	DDPG	59.9	55.7	30.4	69.2	60.7	14.3
	TD3	57.5	52.4	29.9	69.6	62.1	15.9
	TRLF <sub>S</sub>	62.5	63.3	39.8	69.8	64.1	19.1
	$\pi_{maxQ}$	63.5	71.5	53.9	73.9	70.6	21.1
	$\pi_{avg}$	62.3	71.2	60.9	73.2	71.4	23.5
	<b>FusionNet</b>	<b>64.0</b>	65.9	41.6	<b>74.5</b>	73.0	24.9

(b) AF and CC

Data	Algorithm	AF			CC		
		Dice↑	OL↑	OR↓	Dice↑	OL↑	OR↓
HCP	DET	53.4	41.3	10.3	70.9	77.2	41.2
	SAC	54.6	42.4	11.4	70.4	80.4	48.1
	DDPG	50.6	37.9	8.3	65.0	66.2	37.3
	TD3	51.7	39.5	9.6	64.9	66.2	37.2
	TRLF <sub>S</sub>	50.9	38.0	8.2	67.6	67.5	30.9
	$\pi_{maxQ}$	54.8	42.3	10.9	70.4	81.6	50.1
	$\pi_{avg}$	52.3	40.5	12.7	70.1	78.4	46.1
	<b>FusionNet</b>	<b>55.5</b>	43.8	12.3	<b>72.4</b>	81.8	44.8
	TractSeg	70.9	59.5	8.1	76.8	68.5	11.7
TractInferno	<b>FusionNet*</b>	<b>74.1</b>	66.6	13.0	<b>77.4</b>	78.6	23.9
ISM RM	DET	50.0	44.0	35.8	49.7	39.5	19.6
	SAC	52.3	52.4	52.1	54.6	48.3	28.6
	DDPG	46.3	39.3	28.6	49.6	40.4	22.1
	TD3	45.3	39.6	37.6	48.1	38.3	20.9
	TRLF <sub>S</sub>	47.5	43.5	43.2	46.9	37.0	21.1
	$\pi_{maxQ}$	52.7	51.9	47.3	54.2	47.0	30.7
	$\pi_{avg}$	52.1	51.9	49.5	53.3	47.3	31.5
	<b>FusionNet</b>	<b>53.2</b>	51.3	39.1	<b>56.5</b>	50.5	28.8

**Table 3:** Performance comparison (%) for CG, CST/PYT, AF, CC tracts on HCP, TractInferno, and ISMRM datasets. Dice, OL, OR are averaged across test subjects. DET, PROB results from [15]; SAC, DDPG, TD3 from [13] were used to train our network, compared with same specifications. SAC based TRLF<sub>S</sub>[15] trained on EDS. TractSeg and FusionNet\* use TractSeg masks, evaluated on HCP. Best Dice is in bold.

**Note:** While simpler ensembling methods ( $\pi_{maxQ}$  and  $\pi_{Avg}$ ) achieve lower scores than FusionNet, more complex RL ensembling techniques often introduce stability and scalability challenges. TractRLFusion addresses (this) fusion by learning a robust fusion policy in a data-driven manner, which simplifies integration compared to more traditional RL ensemble methods. We illustrate our method with three policies (SAC,

DDPG, TD3) to address the overlap–overreach trade-off, but the framework is modular and can incorporate additional policies to capture broader tracking behaviors.

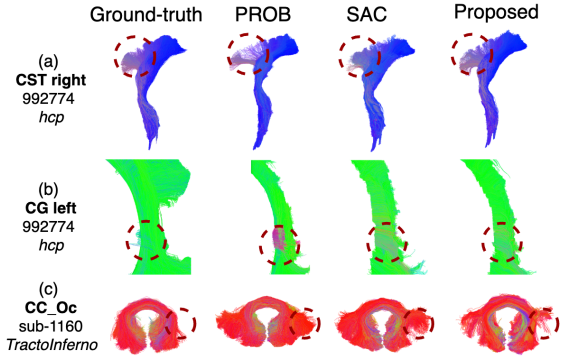


**Fig. 2:** Visualization of the right CST (a) and a segment of the left CG (b) from HCP subject 992774, and the occipital CC (c) from TractInferno subject 1160. The proposed method is compared with PROB, SAC (other top-performers), and ground-truth tracts, with dashed circles marking key regions.

**Ablation Study:** The ablation study underlines the importance of EDS and MCPFT. EDS involves a within-policy and across-policy ( $EDS_{across-\pi}$ ) selection of training trajectories, whereas  $EDS_{across-\pi}$  selects trajectories across different policies using only Q-value. Table 4 reveals that pre-training and finetuning on only EDS (ii) performs worse than ( $EDS_{across-\pi}$ ) (i). Pretraining on coarser  $EDS_{across-\pi}$  and finetuning on EDS (iii) performs the best. Hence FusionNet is trained on data from (iii), followed by MCPFT, whose results in Table 3 show effectively lower OR with higher OL, a desirable outcome in tractography, leading to a higher Dice.

Tract	(i) $EDS_{across-\pi}$ (PT & FT)			(ii) EDS (PT & FT)			(iii) $EDS_{across-\pi}$ PT & EDS FT		
	Dice	OL	OR	Dice	OL	OR	Dice	OL	OR
PYT	70.4	67.3	23.4	58.6	45.7	8.9	70.9	68.3	23.9
CG	59.2	58.6	39.4	42.9	32.1	10.7	61.4	59.5	34.5
AF	47.3	39.7	27.3	23.3	14.4	5.3	48.7	43.5	38.9
CC	67.7	74.1	44.2	60.6	50.3	14.9	68.6	70.2	36.4

**Table 4:** Mean (%) FusionNet scores on TractInferno test data comparing pretraining (PT) & finetuning (FT) strategies.

#### 4. CONCLUSION

**TractRLFusion** enables efficient and effective white matter tracking by fusing complementary strengths of different actor-critic frameworks. Our ablation studies highlight the effectiveness of the proposed two-stage data curation, where a strong baseline policy is first developed using a combination of broad and anatomically-aware data selection (EDS), and subsequently refined through the MCPFT process. TractRLFusion demonstrates strong **generalization**, being trained solely on TractInferno and evaluated on HCP and ISMRM. Finally, powered by **FusionNet**, **TractRLFusion** lays the groundwork for a foundational tractography model with the

potential to extend across additional datasets and integrate diverse specialized policies, advancing the field of White Matter Tractography.

## 5. COMPLIANCE WITH ETHICAL STANDARDS

This study used open-access human data from TractoInferno [20] and the Human Connectome Project [27] in accordance with their licenses, and publicly available phantom data from the ISMRM 2015 Tractography Challenge [29].

## 6. ACKNOWLEDGMENTS

This work was supported by SERB Core Research Grant Project No: CRG/2020/005492, IIT Mandi.

## References

- [1] PJ Basser, S Pajevic, et al., “In vivo fiber tractography using dt-mri data,” *Magnetic resonance in medicine*, vol. 44, no. 4, pp. 625–632, 2000.
- [2] Walid I Essayed et al., “White matter tractography for neuro-surgical planning: A topography-based review of the current state of the art,” *NeuroImage: Clinical*, vol. 15, 2017.
- [3] Peter J Basser, “Fiber-tractography via diffusion tensor mri (dt-mri),” in *Proceedings of the 6th Annual Meeting ISMRM, Sydney, Australia*, 1998, vol. 1226, p. 14.
- [4] Guang Cheng et al., “Tractography from hardi using an intrinsic unscented kalman filter,” *IEEE transactions on medical imaging*, vol. 34, no. 1, pp. 298–305, 2014.
- [5] Jeffrey I Berman et al., “Probabilistic streamline q-ball tractography using the residual bootstrap,” *Neuroimage*, vol. 39, no. 1, pp. 215–222, 2008.
- [6] Marco Reisert et al., “Global fiber reconstruction becomes practical,” *Neuroimage*, vol. 54, no. 2, pp. 955–962, 2011.
- [7] Kurt G Schilling et al., “Challenges in diffusion mri tractography—lessons learned from international benchmark competitions,” *MRI*, vol. 57, pp. 194–209, 2019.
- [8] Koji Kamagata et al., “Advancements in diffusion mri tractography for neurosurgery,” *Investigative Radiology*, vol. 59, no. 1, pp. 13–25, 2024.
- [9] Peter F Neher et al., “A machine learning based approach to fiber tractography using classifier voting,” in *MICCAI 2015, Proceedings, Part I 18*. Springer, 2015, pp. 45–52.
- [10] Philippe Poulin et al., “Learn to track: deep learning for tractography,” in *MICCAI 2017, Part I 20*. Springer, 2017, pp. 540–547.
- [11] Itay Benou et al., “Deeptract: A probabilistic deep learning framework for white matter fiber tractography,” in *MICCAI, 2019*. Springer, 2019, pp. 626–635.
- [12] Antoine Théberge et al., “Track-to-learn: A general framework for tractography with deep reinforcement learning,” *MIA*, vol. 72, pp. 102093, 2021.
- [13] Antoine Théberge et al., “What matters in reinforcement learning for tractography,” *MIA*, vol. 93, pp. 103085, 2024.
- [14] Antoine Théberge et al., “Tractoracle: towards an anatomically-informed reward function for rl-based tractography,” in *MICCAI*. Springer, 2024, pp. 476–486.
- [15] A Joshi et al., “Tract-rlformer: A tract-specific rl policy based decoder-only transformer network,” in *ICPR*. Springer, 2024, pp. 258–275.
- [16] TP Lillicrap, “Continuous control with deep reinforcement learning,” *arXiv preprint arXiv:1509.02971*, 2015.
- [17] Teodor V Marinov et al., “Offline imitation learning from multiple baselines with applications to compiler optimization,” *arXiv preprint arXiv:2403.19462*, 2024.
- [18] S Fujimoto et al., “Addressing function approximation error in actor-critic methods,” in *ICML*. PMLR, 2018, pp. 1587–1596.
- [19] Tuomas Haarnoja et al., “Soft actor-critic: Off-policy maximum entropy deep reinforcement learning with a stochastic actor,” in *ICML*. PMLR, 2018, pp. 1861–1870.
- [20] Philippe Poulin et al., “Tractoinferno-a large-scale, open-source, multi-site database for machine learning dmri tractography,” *Scientific Data*, vol. 9, no. 1, pp. 725, 2022.
- [21] Fang-Cheng Yeh et al., “Population-averaged atlas of the macroscale human structural connectome and its network topology,” *Neuroimage*, vol. 178, pp. 57–68, 2018.
- [22] Yang Li, Ma, et al., “Farthest streamline sampling for the uniform distribution of forearm muscle fiber tracts from diffusion tensor imaging,” *arXiv preprint arXiv:2306.13969*, 2023.
- [23] Alec Radford et al., “Improving language understanding by generative pre-training,” 2018.
- [24] Etienne St-Onge et al., “Fast streamline search: An exact technique for diffusion mri tractography,” *Neuroinformatics*, vol. 20, no. 4, pp. 1093–1104, 2022.
- [25] Francois Rheault, “Population average atlas for recobundlesx,” May 2023.
- [26] J-Donald Tournier et al., “Mrtrix: diffusion tractography in crossing fiber regions,” *International journal of imaging systems and technology*, vol. 22, no. 1, pp. 53–66, 2012.
- [27] J Wasserthal et al., “Tractseg-fast and accurate white matter tract segmentation,” *NeuroImage*, vol. 183, pp. 239–253, 2018.
- [28] Jeremi Levesque, Antoine Théberge, Maxime Descoteaux, and Pierre-Marc Jodoin, “Exploring the robustness of tractoracle methods in rl-based tractography,” *Medical Image Analysis*, p. 103743, 2025.
- [29] Klaus H Maier-Hein et al., “The challenge of mapping the human connectome based on diffusion tractography,” *Nature communications*, vol. 8, no. 1, pp. 1349, 2017.